Journal of Petroleum Science and Engineering 179 (2019) 1037–1045

Contents lists available at ScienceDirect

Journal of Petroleum Science and Engineering

journal homepage: www.elsevier.com/locate/petrol

Controls of CO_2–N_2 gas flood ratios on enhanced shale gas recovery and ultimate CO_2 sequestration

Ziyan Li[a,*], Derek Elsworth[a,b]

[a] Department of Energy and Mineral Engineering, EMS Energy Institute, and G3 Center, The Pennsylvania State University, University Park, PA, USA
[b] Department of Geosciences, The Pennsylvania State University, University Park, PA, USA

ARTICLE INFO

Keywords:
CO_2-Enhanced shale gas recovery
N_2- enhanced shale gas recovery
Adsorption and desorption
CO_2 sequestration
Permeability evolution

ABSTRACT

Primary production of less than 25% of original gas in place (OGIP) may be elevated by enhanced shale gas recovery (ESGR) using either pure CO_2 or N_2 as injected stimulants. Alternatively, injecting mixtures of CO_2 and N_2 may potentially optimize recovery of natural gas and beneficially sequester CO_2. We develop a dual-porosity, dual-permeability finite element (FEM) model coupled with multi-component gas flow and sorption behavior to 1) explore the evolution of sorption-induced strain resulting from competitive adsorption and its influence on the matrix and fracture permeability; 2) define cumulative production of CH_4 and 3) evaluate the amount of CO_2 sequestered in the reservoir; Results show that pure-CO_2 injection can increase shale gas recovery by ~20%. Conversely, pure-N_2 injection can increase shale gas recovery by ~80%. Injecting mixtures of CO_2 and N_2 can increase shale gas recovery between these end-member magnitudes of ~20%–~80% depending on the gas composition. We show that a higher proportion of CO_2 in the injected CO_2–N_2 mixture will result in the decreased recovery of shale gas. However, at the same injection pressure, injecting CO_2–N_2 mixtures with a higher proportion of CO_2 does not always result in more CO_2 sequestered in the reservoir. Indeed, when the CO_2 injection ratio is > 70%, as explored in this study, increasing the CO_2 injection ratio will result in less CO_2 sequestered. This is because, as the CO_2–N_2 gas ratio increases, shale gas recovery decreases and results in more CH_4 left in the reservoir to compete with CO_2 for sorption sites and finally resulting in less CO_2 sequestered.

1. Introduction

Shale gas is methane trapped within a macro- (fracture network) or micro-porosity system (pores) and adsorbed to organic matter (Mecklenburg, 2009). Gas-producing shales are generally rich in Kerogen source, commonly reaching 10% by weight for North American shale gas plays (Kang et al., 2011). Typically 20–85% of the total shale gas-in-place (GIP) is adsorbed to the organic material (Freeman et al., 2014). Despite the combination of horizontal drilling and hydraulic fracturing to create unconventional reservoirs and release the gas (Stevens, 2012) only ~25% (~1161tcf) of the shale gas is technically recoverable of the total estimated reserve of 4644 tcf (Cooper et al., 2016). This suggests a need for improved methods of recovery to access the remaining 75% of this substantial reserve.

The key processes of gas transport during primary production are shown in Fig. 1 (Kalantari-Dahaghi, 2010). When gas is first produced, the pressure in the fracture system declines rapidly prompting desorption as free gas into the matrix and then into the fractures. This free gas is then transported by advection due to the total pressure gradient in the fracture. Injecting CO_2 or N_2 to enhance shale gas recovery (ESGR) is feasible since both can increase the pressure gradient to overcome the extremely low permeability and free the adsorbed gas in the matrix, albeit *via* different mechanisms. Gas adsorption in gas shale typically follows a monolayer adsorption Langmuir isotherm. With this, N_2, CH_4, and CO_2 are preferentially adsorbed on shale in the ratio 2:3:15 (Nuttall et al., 2013; Vermylen, 2011). Injecting a higher affinity gas, such as CO_2, is a practical method to improve recovery because the organic matter in shales has both a large surface area and a greater sorption affinity for CO_2 relative to CH_4 (Nuttall et al., 2013). This both desorbs the lower affinity CH_4 from the kerogen but also has the additional benefit of sequestering CO_2. Conversely, injecting lower affinity N_2 lowers the partial pressure of CH_4 and promotes CH_4 desorption while simultaneously retaining high N_2 pressures that dilate the reservoir rock and potentially increase permeability. As both N_2 and CO_2 can, in theory, enhance shale gas recovery, injecting an optimal mixture of N_2 and CO_2 may combine the advantages of each to maximize their positive impact on ESGR. The source of the N_2–CO_2 mixture could be the flue gas, which is the combustion exhaust waste produced by

* Corresponding author.
E-mail address: ziyan@psu.edu (Z. Li).

https://doi.org/10.1016/j.petrol.2019.04.098
Received 5 December 2018; Received in revised form 19 April 2019; Accepted 28 April 2019
Available online 03 May 2019
0920-4105/

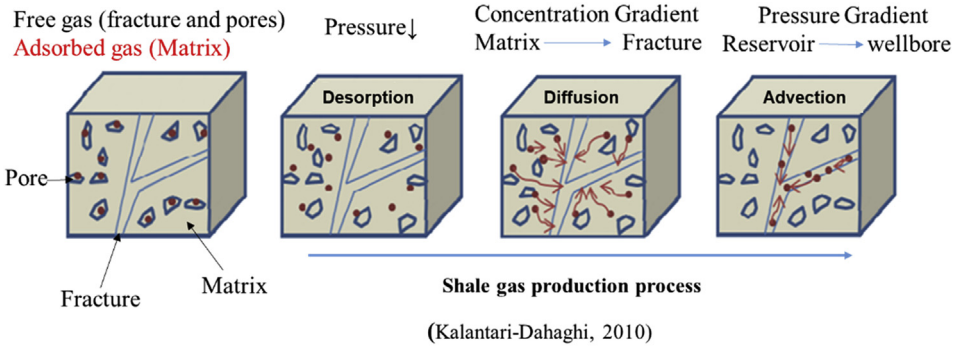

Fig. 1. Transport processes of adsorbed gas during primary production.

thermal power plants. Using a CO_2–N_2 mixture from flue gas can potentially achieve both ESGR and CO_2 sequestration, thus increasing the efficiency of natural gas production and potentially minimizing CO_2 separation effort and cost. Probing for such an optimal injection ratio, and its impact on ESGR and CO_2 sequestration is an important undefined issue and the primary goal of this work.

Currently, EGR in shale gas reservoirs using CO_2 is still at a preliminary stage. At least two pilot projects for EGR are known. The first pilot project worldwide (K12–B) is located in the Dutch sector of the North Sea, where CO_2 was reinjected into the same reservoir following initial gas production and monitored for ~6 years. (Vandeweijer et al., 2011). This exhibited no unexpected problems (Kühn et al., 2014). The Otway pilot site in Victoria, Australia, demonstrated that CO_2 could be safely sequestered in a depleted gas reservoir (Jenkins et al., 2012). No relevant data appear available for N_2 injection. Compared with field demonstrations, numerical modeling enables the simulation of various CO_2-ESGR strategies, such as continuous injection, pulsed injection and huff-and-puff methods at reduced expense and allowing mechanisms and system sensitivity to be effectively determined. A feasibility study of CO_2 ESGR and sequestration (Kalantari-Dahaghi, 2010) clarified the most sensitive parameters impacting shale gas production to be natural fracture permeability, the matrix to fracture coupling factors, shale gas content, matrix permeability and then matrix porosity. Studies comparing CO_2-driven ESGR with sequestration versus re-fracturing treatment of horizontal wells in depleted reservoirs (Eshkalak et al., 2014) showed re-fracturing to be more efficient since refracturing creates a larger effective drainage area and results in increased CH_4 desorption. This is consistent with previous work identifying that fracture permeability exerts the dominant impact on CO_2 ESGR. Reservoir modeling of Devonian gas shales in eastern Kentucky has evaluated the impact of continuous CO_2 injection and huff-and-puff production for both ESGR and CO_2 storage potential (Schepers et al., 2009). This has shown that full-field continuous CO_2 injection is potentially successful, with a ~7%–26% increase in recovery during primary production. However, the huff-and-puff method is limited to ESGR since CO_2 is produced early during the recovery (-puff) period; Studies also showed that continuous CO_2 ESGR, utilizing varying injection pressures (Li and Elsworth, 2014), can enhance gas recovery by ~2%–29%, depending on injection overpressures from 0 to 8 MPa but with a high possibility of CO_2 breakthrough. Pulsed injection was also investigated in this study (Li and Elsworth, 2014), with a ~9% increase in recovery over primary production but without CO_2 breakthrough; Accurately modeling the processes of gas injection or production with complex coupled behaviors such as multicomponent gas flow, competitive sorption, and shale deformation are challenging. In previous studies, a series of single poroelastic (Zhang et al., 2008) or equivalent poroelastic finite element models (Liu et al., 2010) have represented the interactions of multiple processes triggered by injection or production of a single gas in coal. Such models have explored dual poroelastic response for a single gas in coal (Wu et al., 2010; Wu et al., 2011) and have been updated for binary gas flow to investigate the impact of CO_2 injection and differential deformation on CO_2 injectivity under in-situ stress conditions (Chen et al., 2010). Subsequently, all of these models have been combined and applied to enhanced shale gas recovery by CO_2 for both continuous injection and paused and pulsed injection (Li and Elsworth, 2014). In this study, a dual porosity, dual permeability model of multicomponent gas flow incorporating adsorptive behavior is created to represent the processes of ESGR by injecting pure CO_2, pure N_2, and a full spectrum of binary mixtures. Through this we: 1) explore the evolution of sorption-induced strain resulting from competitive adsorption and its influence on the matrix and fracture permeability; 2) define cumulative production of CH_4 and; 3) evaluate the cumulative mass of CO_2 sequestered in the reservoir.

2. Methodology

We develop a dual-porosity, dual-permeability finite element model to simulate the process of flooding with pure-CO_2, pure-N_2 and a full spectrum of their binary mixtures to recover methane. The following introduces key models describing the fluid flow of each of the three species (CO_2, N_2 and CH_4) and how competitive and non-sorbing behavior controls the evolution of permeability in both fracture and matrix.

2.1. Field and constitutive equation

In the following, a set of field equations for gas flow and transport are defined. These field equations are coupled through porosity and permeability models for shale matrix and fractures. These derivations are based on the following assumptions:

1) The shale reservoir is homogeneous, isotropic, and isothermal.
2) Gas in this system is ideal and with constant viscosity.
3) Gas adsorption occurs only in the shale matrix and gas production to the well is restricted to fractures.
4) The presence of a water phase and counter diffusion are not considered.

2.1.1. Multi-component gas transport

Gas mixture transport is based on the time-dependent mass balance equations as,

$$\frac{\partial}{\partial t}(\rho\varphi_k) + \nabla\cdot(\rho\vec{u}_k) = Q \tag{1}$$

where ρ is the density of the gas mixture $[kg/m^3]$, $\varphi$is porosity $[m^3/m^3]$, subscript k represents either matrix (m) or fracture (f). $\vec{u}_k$ is Darcy velocity, and can be expressed as,

$$\vec{u}_f = -\frac{k_f}{\mu}\nabla P \tag{2}$$

$$\vec{u}_m = -\frac{k_m}{\mu}\nabla P \tag{3}$$

where Q represents the mass flux transfer between matrix and fracture adjusted by a shape factor ω and could be a source (+) or sink (−) term, depending on the sign.

$$Q = \omega\nabla\cdot\left(\rho\left(-\frac{k_m}{\mu}\nabla(P_f - P_m)\right)\right) \tag{4}$$

where k_m and $k_f$is the permeability of matrix and fracture$[m^2]$, is the fluid dynamic viscosity $[Pa{\cdot}s]$, P is the total gas pressure $[Pa]$, ω is the shape factor, controlling drainage rate from matrix to the fracture. The shape factor may be calculated as (Li & Elsworth, 2014),

$$\omega = -\frac{3\pi}{a^2} \tag{5}$$

Where a is the fracture spacing.

Finally, the governing equation for gas mixture transport can be summarized as,

$$\frac{\partial}{\partial t}(\rho\varphi_k) + \nabla\cdot\left(\rho\left(-\frac{K_k}{\mu}\nabla P\right)\right) = -\frac{3\pi}{a^2}\nabla\cdot\left(\rho\left(-\frac{K_m}{\mu}\nabla P\right)\right) \tag{6}$$

It is noteworthy that P in these equations (eqns. (2)–(4), (6)) are the gas pressure of the total mixture including CH_4, CO_2, and N_2, which is further used to calculate the approximate Darcy velocity field ($\vec{u}_f$and$\vec{u}_m$) of the gas mixture in both the matrix and fracture system - this provides basic fluid motion for advection and diffusion. Each gas component can be considered individually, flowing though this composite velocity field. The mass balance equation can be expressed, combined with the action of advection, diffusion and dispersion and involving the interchange between free and adsorbed gas as,

$$\frac{\partial}{\partial t}(\rho_{k,i}\varphi_k) + \nabla\cdot(\vec{u}_{k,i}{\cdot}\rho_{k,i}) + \nabla\cdot(-(D_{e,i} + D_{D,i})\cdot\rho_{k,i}) = Q \tag{7}$$

where subscript $i$represents one of gas components (CH_4, CO_2, or N_2) in either the matrix (m) or fracture (f).$D_{e,i}$ is the coefficient of effective dispersion $[m^2/s]$and $D_{D,i}$is the coefficient of diffusion $[m^2/s]$.

This equation can be rewrite in the form of concentration as,

$$\frac{\partial c_{k,i}}{\partial t} + \nabla\cdot(\vec{u}_{k,i}{\cdot}c_{k,i}) + \nabla\cdot(-(D_{e,i} + D_{D,i})\cdot c_{k,i}) = -\frac{3\pi}{a^2}\nabla \cdot\left(C_i\cdot\left(-\frac{K_{m,i}}{\mu}\nabla(C_i{\cdot}R{\cdot}T)\right)\right) \tag{8}$$

where$C_{k,i}$ is the concentration of gas component $i[mol/m^3]$, including free-phase gas and adsorbed gas. The concentration of each component of fracture contained in a unit volume of shale can be defined as,

$$C_{k,i} = \phi_f C_{f,i} \tag{9}$$

As we assume gas adsorption occurs only in the shale matrix, the concentration of component is the summation of free gas and adsorbed gas, which can be expressed as,

$$C_{k,i} = \varphi_m C_{m,i} + \frac{\rho_{m,i}\rho_s(1 - \varphi_m - \varphi_f)V_{adsorption,i}}{M_i} \tag{10}$$

where $\rho_s$is the shale density $[kg/m^3]$and $V_{adsorption,i}$is volume adsorbed per unit mass of shale of the component $i[m^3/kg]$. This adsorbed volume may be expressed by the extended Langmuir isotherm (ELI) as,

$$V_{adsorption,i} = \frac{V_{L,i}C_i b'_i}{1 + \sum_{j=1}^{n} C_j b'_j} \tag{11}$$

where $V_{L,i}$is the Langmuir volume constant of species $i[m^3/kg]$, $b'_i$is a variable used to simplified the ELI as,

$$b'_i = \frac{RT}{P_{L,i}}\,[m^3/mol] \tag{12}$$

where R is the universal gas constant.

2.2. Porosity and permeability equations

In this model, porosity and permeability change is mainly controlled by adsorption and desorption behavior. Thus, the sorption-induced strain ($\varepsilon_{sorption}$) plays a vital role in mediating porosity and permeability change and may be evaluated as (Wu et al., 2011),

$$\varepsilon_{sorption} = \sum_{i=1}^{n}\varepsilon_i = \sum_{i=1}^{n}\frac{\varepsilon_{L,i}C_i b'_i}{1 + \sum_{j=1}^{n} C_j b'_j} \tag{13}$$

where $\varepsilon_{L,i}$is the Langmuir strain isotherm of gas species i.

Based on our previous work, the matrix and fracture porosity can be expressed as (Li& Elsworth, 2015),

$$\frac{\varphi_m}{\varphi_{m0}} = 1 - \frac{\alpha}{\varphi_{m0}K}\cdot\frac{1}{\frac{b}{aK_f} + \frac{1}{K}}(\varepsilon_{sorption} - \varepsilon_v) \tag{14}$$

$$\frac{\varphi_f}{\varphi_{f0}} = 1 - \frac{3}{\varphi_{f0} + \frac{3K_f}{K}}(\varepsilon_{sorption} - \varepsilon_v) \tag{15}$$

where $\varphi_{m0}$is initial matrix porosity [−], $\varphi_{f0}$is initial fracture porosity [−], $K$is matrix bulk modulus of the shale$[GPa]$, $K_f$is the modified fracture stiffness$[GPa]$, $b$is fracture aperture$[m]$ and $\varepsilon_v$is the bulk volumetric strain of the shale, which is considered null in this study (although matrix and fracture may differentially strain at the expense of each other). Since all four external boundaries of the model geometry are assumed constrained, the fracture and matrix permeability can be obtained by cubic law and defined as (Li& Elsworth, 2015),

$$\frac{k_m}{k_{m0}} = \left(1 - \frac{\alpha}{\varphi_{m0}K}\cdot\frac{1}{\frac{b}{aK_f} + \frac{1}{K}}(\varepsilon_{sorption} - \varepsilon_v)\right)^3 \tag{16}$$

$$\frac{k_f}{k_{f0}} = \left(1 - \frac{3}{\varphi_{f0} + \frac{3K_f}{K}}(\varepsilon_{sorption} - \varepsilon_v)\right)^3 \tag{17}$$

where $k_{m0}$is initial matrix permeability$[m^2]$, $k_{f0}$is initial fracture permeability$[m^2]$, $\beta$is the compressibility of the shale$[Pa^{-1}]$.

2.2. Model flowchart

An overview of the linkages between flow mechanisms within the model (Fig. 2(a)) shows the solution algorithm and necessary input parameters for the model. Essentially, this comprises the coupling of ensemble multi-component gas transport as a mixture (eqn. (6)) and single gas component transport within the mixture (eqn. (8)). These two processes communicate through the intermediate variables of the Darcy velocity field, gas species concentration, porosity, and permeability in each solution step with the concentration distribution of each species obtained at each iterative time step.

To accurately simulate fluid flow in the shale reservoir, the model is constructed including matrix and fracture systems as separate but overlapping continua, sharing the same geometry and mesh but with their own representative permeability and porosity, as shown in Fig. 2(b) or 2(c). Transport of the gas mixture is represented by applying constant injection and production pressures on the wellbore boundary as shown in Fig. 2(b). Since the wells are assumed only connected to the fracture system, an instantaneous pressure redistribution in the fracture system will lead to a pressure difference between matrix and fracture. This will induce mass transfer between matrix and fracture, calculated from this pressure difference and modulated by the shape factor (eqn. (5)). This defines the Darcy velocity field distribution in both fracture and matrix, which is then used as an intermediate input parameter to calculate the concentration of each specific gas species in the system (eqn. (8)). With the concentration of each species on the injection and production boundary known (Fig. 3.

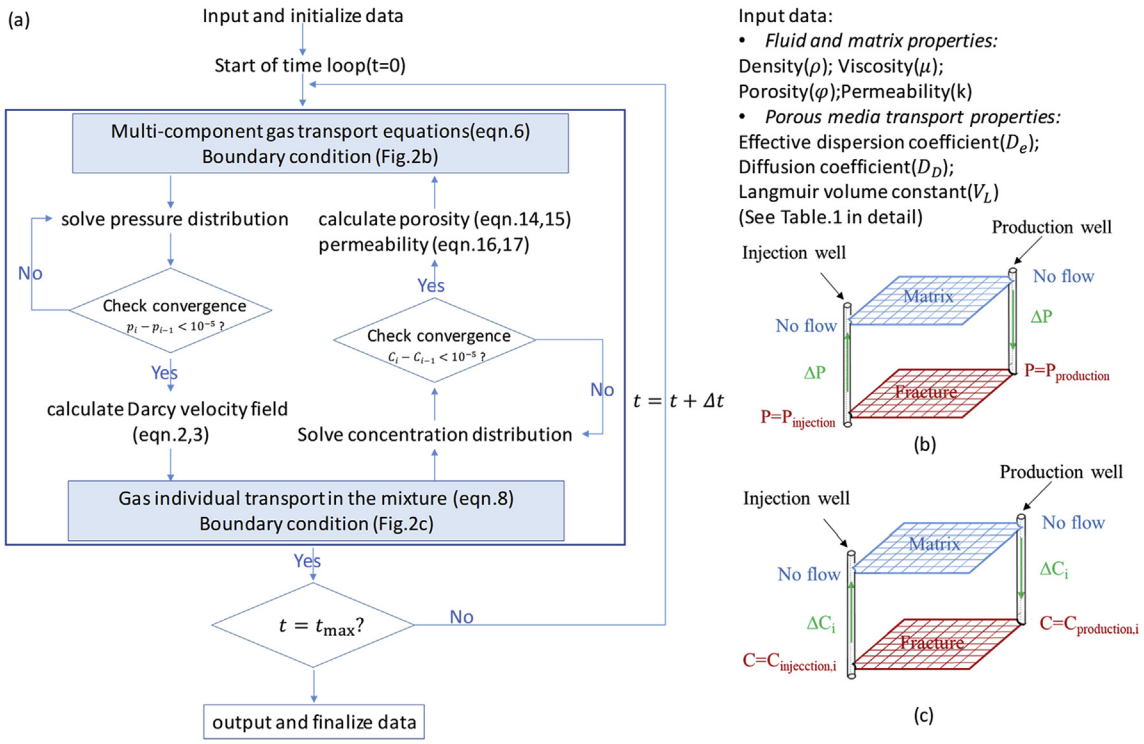

Fig. 2. (a) Core algorithm of the model. The solution is a consecutively updated to represent the processes of gas mixture transport and single gas component transport within the mixture, by updating the intermediate parameters including the Darcy velocity field, the concentration of each species, and porosity and permeability at each time step. (b) The model structure of gas mixture transport with pressure boundary conditions at the injection and production wells both in the matrix and in the fracture system (c). The model structure of single component gas transport in the mixture, with concentration boundary conditions of injection and production wells both in the matrix and in the fracture system for one specific gas species. The linkage between matrix and fracture is also included.

(c)), as calculated from the partial pressure from the ideal gas equation, then concentration of each gas species is updated and new competitive sorption (eqn. (13)), porosity (eqn. (14) and (15)) and permeability (eqn. (16) and (17)) are updated and returned to the gas mixture transport calculation for the next step. The solutions of equations that represent these two processes are continuously and consecutively updated until the gas concentration distribution of each species over time is known.

3. Parametric study

In this section, a numerical model is developed with a well-defined set of parameters. The equations applied in the model have been solved using the commercial simulator COMSOL Multiphysics 5.2, using the finite element method (FEM) to solve the governing partial differential equations (PDEs), numerically. We validate the model against standard stability criteria for transport. The Peclet number and the Courant number are calculated to ensure stable performance by manipulating both element size and time step to guarantee stability.

3.1. Model description

We select a representative portion of a reservoir 200 m in length, 120 m in width and 120 m in depth as shown Fig. 3(a). The initial gas pressure in the reservoir is 30 MPa, representing the pore pressure at a depth of 3000 m. In this study, the three gas components comprise CH_4, CO_2, N_2 at pre-defined initial concentrations in the reservoir of 95%, 4% and 1% in the fracture system and 85%, 14% and 1% in the matrix. The initial partial pressures of one specific gas are set according to its composition: CH_4, CO_2, and N_2 are assigned with initial partial pressures of 28.5 MPa, 1.2 MPa, and 0.3 MPa in the fracture, and 25.5 MPa, 4.2 MPa, 0.3 MPa in the matrix, respectively. The original gas in place

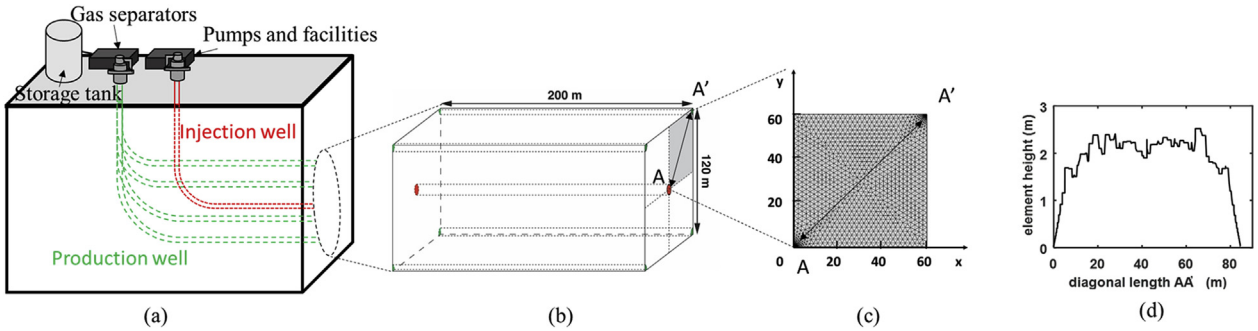

Fig. 3. (a) Schematic of the reservoir showing distribution of horizontal wells. (b) Conceptual model used in the simulation with a specific dimension of 200 m × 120 m × 120 m, and quarter-symmetry simulation model as shaded. AA′ is the diagonal trace between injector (A) and production (A′) well. (c) Mesh used in the simulation as identical for both matrix and fracture as shown in Fig. 2b and c. (d) Triangular element height distribution along the diagonal line AA'.

(OGIP) is evaluated as the total mass of CH_4 per unit volume separately within both fracture and matrix (eqn. (14)) multiplied by reservoir volume. This may also be represented in the form of concentration as in eqn. (15). It is noteworthy that the concentration of CH_4 in the matrix already includes both free and adsorbed CH_4. If this CH_4 is produced in its entirety, the volume of CH_4 under the standard conditions is $3.59 \times 10^{+7}m^3$ (1267 MMscf) as,

$$m_{CH_4} = m_{f,CH_4} + m_{m,CH_4} \tag{18}$$

$$m_{CH_4} = \left(C_{f,CH_4} + C_{m,CH_4}\right) \times M_{CH_4} \tag{19}$$

The reservoir is accessed by 5 horizontal wells that are produced over 30 years. The well pattern is a regular (horizontally aligned) five-spot pattern with one injection well in the center flanked by four production wells at the corners (Fig. 3(a)). The symmetry of the flow regime in this system allows representation by a single quadrant of the reservoir, taken in the vertical plane (Fig. 3(b)). This one-quarter section is represented by the gray shaded region (Fig. 3(b)) with the mesh distribution shown in Fig. 3(b). The trace AA' is the diagonal line of the target gas flow area from the injection well to a production well.

For these parametric studies, CO_2 and N_2 are injected either individually or as a mixture in various ratios and at different injection pressure schemes. These summarized schemes are: (1) Withdrawal only, with no injection (primary production), (2) Injection at 4 MPa overpressure, and (3) Injection at 8 MPa overpressure above an initial reservoir pressure of 30 MPa. Each simulation runs for 30 years allowing CH_4 recovery and CO_2 sequestration are evaluated. The initial parameters used in the simulation and their source are shown in Table 1, below.

3.2. Model validation

The numerical model developed in section 3.1 is applied here to investigate the controls of CO_2–N_2 gas flood ratios on enhanced shale gas recovery and ultimate CO_2 sequestration for an ideal representative reservoir. Reasonable computational limits are placed on both memory and runtime and calculations are conducted using triangular elements with the minimum triangle height distribution showing in Fig. 3(d). In this section, Peclet and Courant numbers are calculated along the diagonal line (AA') with time to test whether or not element size and time step is stable and reasonable. The Peclet number is a dimensionless number that can relate the effectiveness of mass transport by advection to mass transport by diffusion. It is defined as,

$$Pe = \frac{N_{advection}}{N_{diffusion}} = \frac{t_{diffusion}}{t_{advection}} = \frac{L^2/D_h}{L/U} = \frac{LU}{D_h} \tag{20}$$

where L is a characteristic length, U is Darcy velocity magnitude, and D_h is the sum of characteristic diffusion and dispersion coefficient.

When the Peclet number is less than one, it is diffusion dominant in the mass flux, and when the Peclet number is greater than one, the effects of convection exceed those of diffusion in determining the overall mass flux. If the Peclet number is greater than 10 to 100 that can cause problems with the numerical stability. The Peclet number across the diagonal line of the representative quarter of the reservoir is shown in Fig. 4(a). The Peclet number is relatively small at both injection or production well relative to that in the middle because meshes are much denser at the well to describe the geometry of the well, as shown in Fig. 3(d). It is important to note that a higher mesh resolution results in a more accurate solution but more computational effort. To find a balance between accuracy and effort, we accept the current mesh distribution as shown in Fig. 3(d), which finally leads to some regions with Peclet numbers reaching 10. However, COMSOL uses upwind weighting in these regions to reduce oscillations at the expense of some numerical dispersion.

The Courant number is a measure of how much information traverses a computational grid cell in a given time, which is defined as

$$C = \frac{U\Delta t}{\Delta x} \tag{21}$$

where Δt is the time-step of the numerical model (Δt = 86400s in this model), and Δx is the element length in the numerical model.

The Courant number should be restricted to less than unity to guarantee a stable solution. The Courant number across the diagonal line of the symmetric quarter domain of the reservoir is shown in Fig. 4(b) – guaranteeing that it is less than unity. These, coupled with other validation exercises, guarantee the veracity of the resulting model.

Table 1
Modeling parameters used in the simulation.

	Value	Unit	Reference
Initial reservoir temperature (T_0)	300	R	Li & Elsworth (2014)
Initial reservoir pressure (P_0)	30×10^3	Pa	Li & Elsworth (2014)
Initial porosity of matrix (φ_m)	0.041	–	Strickland et al. (2011)
Initial porosity of fracture (φ_f)	0.007	–	Wang & Reed (2009)
Initial permeability of matrix (k_m)	2.17×10^{-19}	m^2	Strickland et al. (2011)
Initial permeability of fracture (k_f)	2.27×10^{-17}	m^2	Strickland et al. (2011)
fracture aperture (b)	5×10^{-4}	m	Li & Elsworth (2014)
fracture spacing (a)	0.025	m	Li & Elsworth (2014)
Density of shale (ρ)	2500	Kg/m^3	Li & Elsworth (2014)
Young's modulus of shale (E_s)	32.75×10^9	Pa	Goodway et al. (2006)
Young's modulus of shale grain (E_g)	40.54×10^9	Pa	Vermylen (2011)
Poisson's ratio of shale (ν)	0.235	–	Goodway et al. (2006)
CH_4 dynamic viscosity (μ_{CH_4})	1.15×10^{-5}	Pa·s	Wu et al. (2011)
CO_2 dynamic viscosity (μ_{CH_2})	1.6×10^{-5}	Pa·s	Wu et al. (2011)
N_2 dynamic viscosity (μ_{N_2})	1.75×10^{-5}	Pa·s	Vermylen (2011)
CH_4 Langmuir pressure constant (P_{L,CH_4})	6.9×10^3	Pa	Vermylen (2011)
CO_2 Langmuir pressure constant (P_{L,CO_2})	2.51×10^3	Pa	Vermylen (2011)
N_2 Langmuir pressure constant (P_{L,N_2})	8×10^3	Pa	Vermylen (2011)
CH_4 Langmuir volume constant (V_{L,CH_4})	1.05×10^{-3}	m^3/Kg	Vermylen (2011)
CO_2 Langmuir volume constant (V_{L,CO_2})	4.93×10^{-3}	m^3/Kg	Vermylen (2011)
N_2 Langmuir volume constant (V_{L,N_2})	2.5×10^{-3}	m^3/Kg	Vermylen (2011)
CH_4 Langmuir volumetric strain constant (ε_{L,CH_4})	8.1×10^{-4}	–	Vermylen (2011)
CH_4 Langmuir volumetric strain constant (ε_{L,CO_2})	3.6×10^{-3}	–	Vermylen (2011)
CH_4 Langmuir volumetric strain constant (ε_{L,N_2})	7.5×10^{-4}	–	Vermylen (2011)

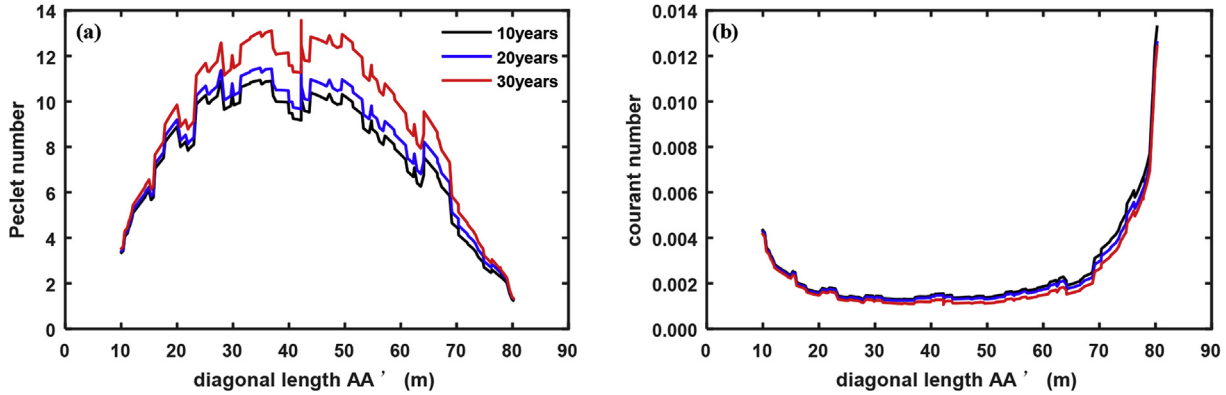

Fig. 4. (a) Peclet number along diagonal AA′ at 10 years, 20 years and 30 years. (b) Courant number along diagonal AA′ at 10 years, 20 years and 30 years.

4. Results and discussion

The dual-porosity, dual-permeability finite element (FEM) model coupled with multi-component gas flow and sorption behavior is used to 1) explore the evolution of sorption-induced strain resulting from competitive adsorption and its influence on the matrix and fracture permeability; 2) define cumulative production of CH_4; 3) and to describe the mass of CO_2 sequestered in the reservoir;

4.1. Permeability evolution

Matrix permeability change is characterized by the matrix permeability ratio. This is defined as the matrix permeability divided by the initial matrix permeability. The fracture permeability ratio is defined in the same way.

Pure N2 and pure CO2 are separately injected under either 4 MPa (solid line) or 8 MPa (dashed line) overpressures for ESGR. The matrix and fracture permeability ratio are represented in Fig. 5 over 10-years of injection. The matrix and fracture permeability ratio under pure N2 injection and pure CO2 injection is mainly focused local to injection (left hand side of each figure). This is because the injected N2 will desorb CH4 by lowering its partial pressure. CH4 desorption, combined with N2 injection, results in matrix shrinkage and complementary fracture widening. Conversely, injected CO2 will displace CH4 due to its higher adsorption affinity. CO2 adsorption and CH4 desorption then results in matrix swelling and complementary fracture shrinkage (closure). Matrix permeability ratio decreases (Fig. 5(a) and (c)) and fracture permeability ratio increases (Fig. 5(b) and (d)) at the production well (right hand side of each figure), as a result of reduced pressure of CH4 as production desorbs CH4 that induces matrix shrinkage and complementary fracture widening.

The overall effect of pure CO_2 or pure N_2 ESGR on permeability is

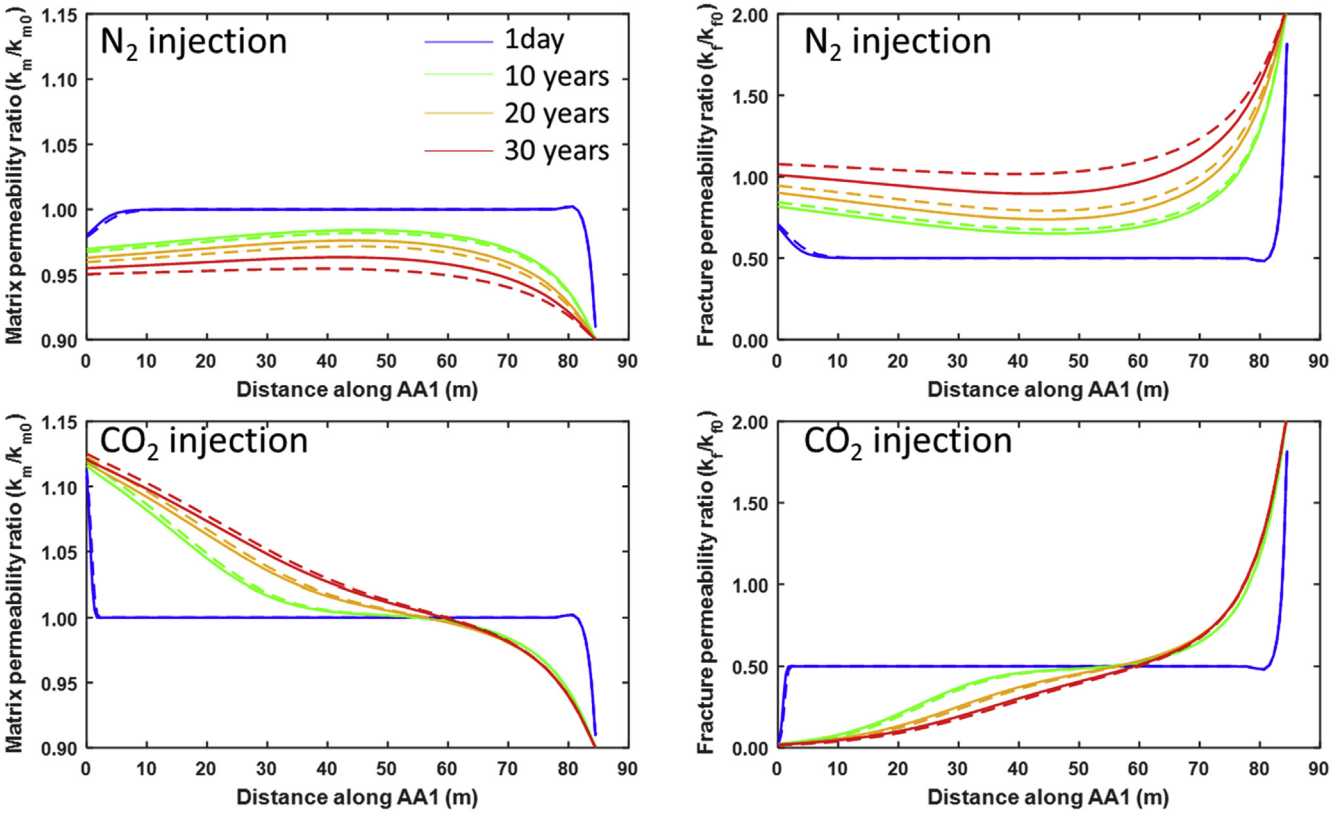

Fig. 5. Time history of (a) matrix permeability evolution and (b) fracture permeability evolution resulting from injection of pure N2 as an ESGR stimulant; Time history of (c) matrix permeability evolution and (d) fracture permeability evolution resulting from injection of pure CO2.

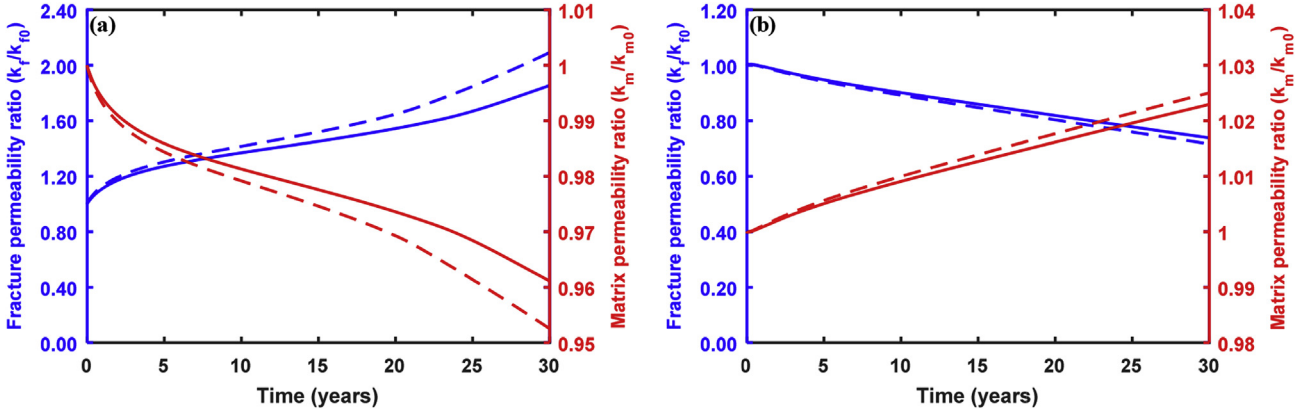

Fig. 6. (a) The evolution of average matrix permeability ratio (K_m/K_{m0}) and fracture permeability ratio (K_f/K_{f0}) under N_2 injection at 4 MPa overpressure (solid line) and 8 MPa overpressure (dashed line). (b) The evolution of average matrix permeability ratio (K_m/K_{m0}) and fracture permeability ratio (K_f/K_{f0}) under CO_2 injection.

apparent in the average matrix and fracture permeability ratio as defined over the entire reservoir: N_2 injection causes a decrease in the average matrix permeability and an increase in the average fracture permeability over time, while CO_2 injection results in the opposite effect (average fracture permeability decreases and average matrix permeability increases), as shown in Fig. 6 (a) and (b).

4.2. Cumulative shale gas production

The cumulative shale gas production under CO_2 injection, N_2 injection, and the spectrum of mixtures of those two gases is shown in Fig. 7(a). The black line shows the primary production, and the blue and the red lines represent the production under pure CO_2 or N_2, respectively. The intermediate responses represent mixtures of N_2 and CO_2 injection in different ratios. It is apparent that both CO_2 and N_2 injection each enhance shale gas recovery, and by different margins. CO_2 injection increases shale gas recovery by ~20% based on primary recovery over 30 years. The production improvement is maybe not as high as expected because CO_2 adsorption results in matrix swelling which decreases fracture permeability and correspondingly impedes production. Injection of pure N_2 also increases shale gas recovery, and in this case by ~80%. This increased efficiency is because N_2 injection lowers the partial pressure of CH_4 in the shale, prompting gas desorption from the matrix and simultaneously induces fracture enlargement – a second mechanism and effect that is the opposite for CO_2 injection. Production decreases with an increased proportion (percentage) of CO_2 in the injected mixture, relative to N_2. This relationship is represented in Fig. 7. (b).

It is concluded from Fig. 7(b) that although pure CO_2 injection can recover more than primary recovery, alone, a higher proportion of CO_2 in the injectate will result in a decreased recovery of CH_4 due to impacts on reduced permeability. Stated differently, increasing pressure is not the only means to achieve higher ESGR production. Instead, lowering the CO_2 ratio in the injected CO_2–N_2 mixture can achieve the same goal.

4.3. CO_2 sequestration

The volume (STP) of CO_2 sequestered versus time is shown in Fig. 8(a) for CO_2–N_2 mixtures in different gas ratios. Observations show that although the CH_4 recovery rate *via* CO_2-ESGR is insensitive to the injection pressure, the mass of CO_2 sequestered is strongly influenced by pressure. Furthermore, at the same injection pressure, injecting CO_2–N_2 mixtures with a higher proportion of CO_2 does not always results in more CO_2 sequestered in the reservoir. For instance, pure CO_2 injection, unexpectedly, results in less sequestered CO_2 than a mixture with 75% CO_2 and 25% N_2. This is due to the influence of permeability change as a result of CO_2 sorption (fracture permeability decreases) relative to that with N_2 where fractures are dilated at high injection pressures.

Focusing on the relationship between CO_2 sequestration and CO_2 injection ratio, it is apparent in Fig. 8. (b) that CO_2 could be sequestered in the reservoir during ESGR only if the CO_2 injection ratio is greater than 20%. Otherwise, the CO_2 would be directly flooded out from the reservoir by N_2 without any sequestration. Additionally, the increase in the amount of CO_2 sequestered with increasing CO_2 proportion is not linear. This likely result since, as the CO_2–N_2 gas ratio increases, shale gas recovery decreases, which leads to more CH_4 left in the reservoir to compete with CO_2 for sorption sites and finally results in less CO_2

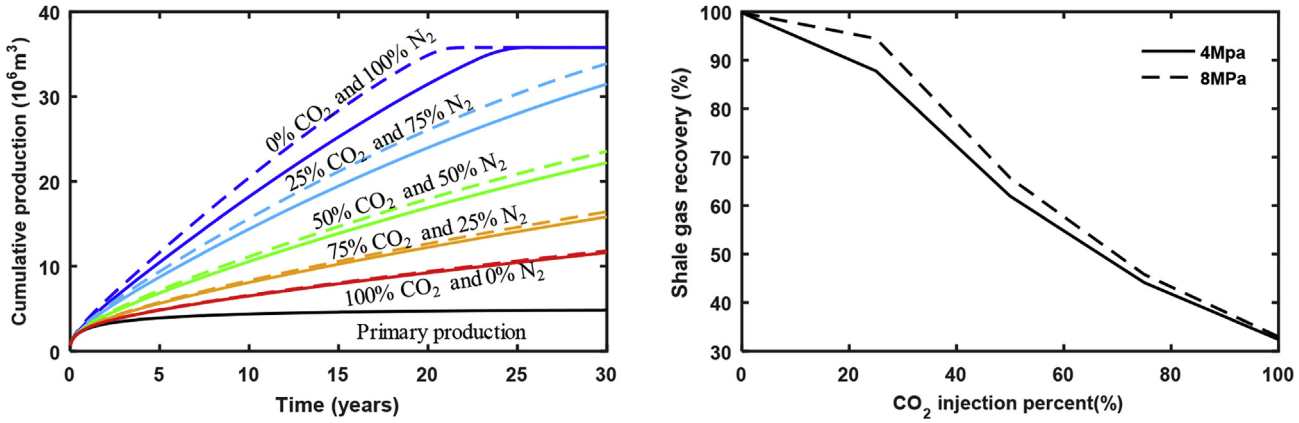

Fig. 7. (a) Cumulative CH4 production vs. time for mixtures of N2 and CO2 injected in different ratios under 4 MPa overpressure injection (solid line) and 8 MPa overpressure (dashed line), relative to primary production without EGR. (b) Relationship between shale gas recovery and CO2 injection ratio.

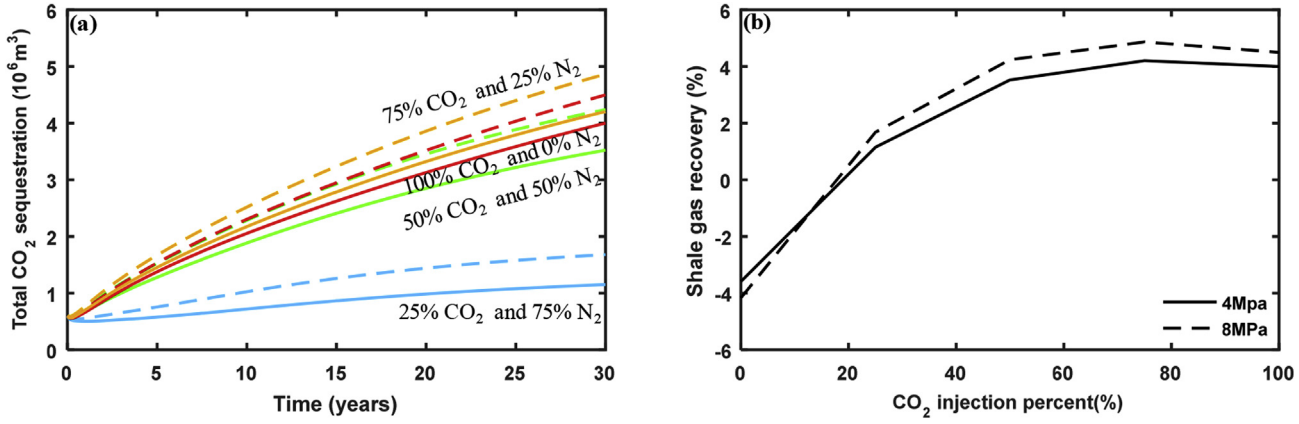

Fig. 8. (a) Total CO2 sequestered with time under injection of N2 and CO2 in different ratios. (b) Percentage of CO2 injected at 4 MPa (solid line) and 8 MPa (dashed line) overpressure.

sequestration. Apparent from Fig. 8(b) is that the optimal CO_2 proportion for CO_2 sequestration is ~80%.

5. Conclusion

This study explores mechanisms of enhanced shale gas recovery (ESGR) using the injection of a spectrum of mixtures of CO_2 and N_2. A finite element dual-porosity, dual-permeability model of multi-component gas flow in porous media is coupled with sorption behavior. Furthermore, the injection of both pure CO_2 and N_2 and as a mixture in different ratios is explored. The following two conclusions are drawn:

1. CO_2 and N_2 can both enhance shale gas recovery, but *via* different mechanisms:
   (1) Injection of CO_2 can increase shale gas recovery since CO_2 has a higher absorbability than CH_4 and thereby CO_2 competitively desorbs CH_4. This can increase the recovery of CH_4 by ~20%, based on primary recovery. This improvement is relatively minor since CO_2 adsorption results in matrix swelling which concomitantly decreases fracture permeability and correspondingly impedes production. Despite this, CO_2 can be used in ESGR where concurrent sequestration of the greenhouse gas will also occur.
   (2) Injection of N_2 in ESGR can also increase shale gas recovery but by a much larger margin of ~80%, since N_2 lowers the partial pressure of CH_4 in shale. This then accelerates desorption of shale gas from the matrix and induces fracture enlargement as a consequence of shrinkage of the shale matrix - due to the lower absorbability of the shale to N_2 with respect to CH_4. Although injection of N_2 as an agent for ESGR has many advantages, it cannot concurrently sequester CO_2 to mitigate greenhouse gas emissions.
2. Injection of pure CO_2 and pure N_2 both have their advantages and disadvantages in ESGR. Injecting an optimal mixture of N_2 and CO_2 may combine the advantages of each gas to maximize their positive impact and minimize their negative impact:
   (1) Injection of N_2 in higher proportions relative to CO_2 improves shale gas recovery since N_2 is more effective in ESGR.
   (2) Enhanced recovery is less sensitive to pressure for CO_2 injection than to N_2. Therefore, increasing injection pressure has an insignificant effect on shale gas recovery when the CO_2 proportion in the injected gas is high.
   (3) Increasing pressure is not the only means to achieve ESGR - instead, increasing the N_2–CO_2 ratio can achieve the same goal.

References

Chen, Z., Liu, J., Elsworth, D., Connell, L.D., Pan, Z., 2010. Impact of CO2 injection and differential deformation on CO2 injectivity under in-situ stress conditions. Int. J. Coal Geol. 81. https://doi.org/10.1016/j.coal.2009.11.009.

Cooper, J., Stamford, L., Azapagic, A., 2016. Shale gas: a review of the economic, environmental, and social sustainability. Energy Technol. 4. https://doi.org/10.1002/ente.201500464.

Eshkalak, M.O., Al-Shalabi, E.W., Sanaei, A., Aybar, U., Sepehrnoori, K., 2014. Simulation study on the CO2-driven enhanced gas recovery with sequestration versus the refracturing treatment of horizontal wells in the U.S. unconventional shale reservoirs. J. Nat. Gas Sci. Eng. 21, 1015–1024. https://doi.org/10.1016/j.jngse.2014.10.013.

Freeman, S., Eddy, S.L., McDonough, M., Smith, M.K., Okoroafor, N., Jordt, H., Wenderoth, M.P., 2014. Active learning increases student performance in science, engineering, and mathematics. Proc. Natl. Acad. Sci. Unit. States Am. 111 (23), 8410–8415. https://doi.org/10.1073/pnas.1319030111.

Goodway, B., Varsek, J., Abaco, C., 2006. Practical applications of P-wave AVO for unconventional gas Resource Plays Part 2: detection of fracture prone zones with Azimuthal AVO and coherence discontinuity. CSEG Recorder (4), 52–64. Retrieved from. http://csegrecorder.com/articles/view/practical-applications-of-p-wave-avo-for-unconventional-gas-resource-plays.

Jenkins, C.R., Cook, P.J., Ennis-King, J., Undershultz, J., Boreham, C., Dance, T., et al., 2012. Safe storage and effective monitoring of CO2 in depleted gas fields. Proc. Natl. Acad. Sci. Unit. States Am. 109 (2), E35–E41. https://doi.org/10.1073/pnas.1107255108.

Kalantari-Dahaghi, A., 2010. Numerical simulation and modeling of enhanced gas recovery and CO 2 sequestration in shale gas reservoirs: a feasibility study. In: SPE International Conference on CO2 Capture, Storage, and Utilization, . https://doi.org/10.2118/139701-MS.

Kang, S.M., Fathi, E., Ambrose, R.J., Akkutlu, I.Y., Sigal, R.F., 2011. Carbon dioxide storage capacity of organic-rich shales. SPE J. (December), 842–855. https://doi.org/https://doi.org/10.2118/134583-PA.

Kühn, M., Nakaten, N., Streibel, M., Kempka, T., 2014. CO2geological storage and utilization for a carbon neutral "power-to-gas-to-power" cycle to even out fluctuations of renewable energy provision. Energy Procedia 63, 8044–8049. https://doi.org/10.1016/j.egypro.2014.11.841.

Li, X., Elsworth, D., 2014. Geomechanics of CO2 enhanced shale gas recovery. J. Nat. Gas Sci. Eng. 26, 1607–1619. https://doi.org/10.1016/j.jngse.2014.08.010.

Liu, J., Chen, Z., Elsworth, D., Miao, X., 2010. Linking Gas-Sorption Induced Changes in Coal Permeability to Directional Strains through a Modulus Reduction ratio.Pdf.

Mecklenburg, C.W., Mecklenburg, T.A., 2009. Modern shale gas development in the United States. Arctic marine fish museum specimens. In: Database Submitted to ArcOD, Institute of Marine Science, University of Alaska Fairbanks by Point Stephens Research, PO Box, 210307(April), second ed. .

Nuttall, B.C., Godec, M.L., Butsch, R.J., Riestenberg, D.E., 2013. Assessment of CO 2 Enhanced Gas Recovery in Shale Gas Reservoirs (Preliminary)*. pp. 80296 September 2012.

Schepers, K.C., Nuttal, B., Oudinot, A.Y., Gonzalez, R., 2009. Reservoir modeling and simulation of the devonian gas shale of eastern Kentucky for enhanced gas recovery and CO 2 storage. In: SPE International Conference on Capture, Storage, and Utilization, pp. 10–11. https://doi.org/10.2118/126620-MS.

Stevens, P., 2012. The 'Shale Gas Revolution': Developments and Changes. Chatham House, pp. 2–3.

Strickland, R., Purvis, D., Group, T.S., Blasingame, T., Texas, A., 2011. SPE 144357 practical aspects of reserve determinations for shale gas. Area 12–16.

Vandeweijer, V., van der Meer, B., Hofstee, C., Mulders, F., D'Hoore, D., Graven, H., 2011. Monitoring the CO2 injection site: K12-B. Energy Procedia 4, 5471–5478. https://doi.org/10.1016/j.egypro.2011.02.532.

Vermylen, J.P., 2011. Geomechanical Studies of the Barnett Shale, Texas, USA, vol.125. pp. 143 May.

Wang, F.P., Reed, R.M., 2009. Pore networks and fluid flow in gas shales. SPE Annual,

SPE 124253, 8. https://doi.org/10.2118/124253-MS.
Wu, Y., Liu, J., Chen, Z., Elsworth, D., Pone, D., 2011. A dual poroelastic model for CO2-enhanced coalbed methane recovery. Int. J. Coal Geol. 86. https://doi.org/10.1016/j.coal.2011.01.004.
Wu, Y., Liu, J., Elsworth, D., Chen, Z., Connell, L., Pan, Z., 2010. Dual poroelastic response of a coal seam to CO2 injection. International Journal of Greenhouse Gas Control 4. https://doi.org/10.1016/j.ijggc.2010.02.004.
Zhang, H., Liu, J., Elsworth, D., 2008. How sorption-induced matrix deformation affects gas flow in coal seams: a new FE model. Int. J. Rock Mech. Min. Sci. 45. https://doi.org/10.1016/j.ijrmms.2007.11.007.